A Viscoelastic Theory of Turbulent Fluid Permeated with Fibril Magnetic Fields

D. W. Longcope[1]

Department of Physics, Montana State University,
Bozeman, MT 59717

dana@solar.physics.montana.edu

and

T.C.B. McLeish[1]

Department of Physics and Astronomy,
University of Leeds, Leeds LS2 9JT, UK

and

G.H. Fisher[1]

Space Sciences Laboratory, University of California
Berkeley, CA 94720-7450

ABSTRACT

The solar convection zone is a turbulent plasma interacting with a magnetic field. Its magnetic field is often described as fibrillar since it consists of slender flux tubes occupying a small fraction of the total volume. It is well-known that plasma flow will exert a force on these magnetic fibrils, but few models have accounted for the back-reaction of the fibrils on the flow. We present a model in which the back-reaction of the fibrils on the flow is manifest as viscoelastic properties. On short time scales the fibrils react elastically with a shear modulus proportional to their overall magnetic energy density. On longer times scales they produce an effective viscosity resulting from collective aerodynamic drag. The viscosity due to flux tubes in the solar convection zone can be comparable to that attributed to turbulence there. These forces might have observable effects on the convection zone flows.

Subject headings: Sun: interior — convection — Sun: magnetic fields — turbulence — MHD — magnetic fields

---

[1]Institute for Theoretical Physics, University of California, Santa Barbara, CA 93106

1. Introduction

The interaction between a turbulent plasma and a magnetic field is a problem of long standing in astrophysics. A kinematic treatment of this problem studies the evolution of the magnetic field in the presence of a prescribed plasma flow. A well-known result of such an approach is the α-effect, whereby kinetic helicity in a turbulent flow leads to amplification of the magnetic field; the system is a magnetic dynamo. A typical derivation invokes *mean-field electrodynamics* in which the magnetic field is decomposed into a dominant smooth component plus small-scale, small-amplitude fluctuations (Moffatt 1978; Krause and Rädler 1981) representing turbulence. Averaging the magnetic induction equation over the rapidly fluctuating velocity yields the α-effect.

Were the α-effect to persist it is believed that the amplified magnetic field would become strong enough to affect the fluid flow, violating the kinematic assumption. This hypothetical "back-reaction" on the flow by the magnetic field has been the subject of several investigations some of which predict significant back-reaction even by very weak fields (Vainshtein and Cattaneo 1992; Kulsrud and Anderson 1992; Bhattacharjee and Yuan 1995). If the back reaction has the effect of quenching the dynamo action before it can generate a significant field, then these results cast serious doubt on the viability of the either the α-effect or mean field electrodynamics, when confronted with the observed existence of relatively strong dynamo-generated magnetic fields.

The solar convection zone is undoubtedly the best known and most thoroughly studied astrophysical example of a turbulent plasma with a magnetic field. Where it is most easily measured, at the solar surface, the magnetic field is highly intermittent and seems poorly approximated by mean-field electrodynamics. It is perhaps more accurate to describe the photosphere as a *fibril field*, in light of its concentration into features ranging from active regions on the largest scale down to $\sim 10^{17}$ Mx flux elements (Stenflo 1973) at the smallest scales yet resolved. Many properties of sunspots and active regions have been successfully interpreted by describing these surface phenomena as the manifestations of strands of magnetic flux, called *flux tubes*, extending through all or most of the convection zone (Parker 1955).

In its idealized form a fibril field is one where all magnetic field occurs in such discrete flux tubes, each separated by a sharp interface from a surrounding field-free plasma (Parker 1955; Roberts and Webb 1978; Spruit 1981). This assumed field structure stands in contrast to *continuum* models, such as mean-field electrodynamics or full magnetohydrodynamics (MHD), where $\mathbf{B}(\mathbf{x})$ is a smooth function, vanishing only at isolated points or in small regions. Theoretical arguments predict that high Reynolds number turbulence will concentrate the magnetic field into fibrils with relatively small filling factor (Weiss 1966; Parker 1984). Numerical solutions of nonlinear MHD equations, at the highest

Reynolds numbers practical, have confirmed this tendency for concentration, but not to the extent that flux tubes become truly isolated (Nordlund *et al.* 1992; Matthews *et al.* 1995; Brummell *et al.* 2002). Moreover, very sensitive measurements show that the regions surrounding photospheric flux tubes are not truly field-free (Lin and Rimmele 1999). Thus the fibril state appears to be an idealization which is not likely to occur in reality. Nevertheless, its highly intermittent nature suggests that the solar magnetic field might be more reasonably approximated as a fibril field than as a field whose small-scale fluctuations are perturbations on a smooth component.

Dynamical equations for a single flux tube follow from ideal MHD applied to the plasma *inside* the tube (Roberts and Webb 1978; Spruit 1981). The results are a set of equations, called the *thin flux tube model*, describing the dynamics of a one-dimensional space-curve (the tube's axis) which are formally similar to the equations of motion for a buoyant elastic string. Versions of the thin flux tube equations typically applied to the solar convection zone include the effects of gravity (i.e. buoyancy), magnetic tension and the Coriolis force. The external medium couples across the tube's interface through an aerodynamic drag force (Parker 1979; Choudhuri and Gilman 1987), much as it would to a string at high Reynolds number. In a stationary atmosphere this drag counter-acts the buoyancy so an active region flux tube rises to the solar surface at its terminal velocity. Solutions of this case have shown remarkable agreement with the observed properties of active regions and sunspot groups (D'Silva and Choudhuri 1993; Fan *et al.* 1993; D'Silva and Howard 1993; Fan *et al.* 1994; Caligari *et al.* 1995). Rising through a medium with turbulent velocity a tube's axis develops perturbations which match the statistical scatter present in the same observations (Longcope and Fisher 1996; Longcope *et al.* 1998; Longcope and Choudhuri 2002).

To date, fibril fields have been studied primarily in the kinematic regime where they are affected by the unmagnetized background but exert no back-reaction on it. It seems unlikely that a single flux tube would significantly alter flows in the convection zone, making the kinematic limit a reasonable one. The combined forces of all the flux tubes in the convection zone might, however, be enough to affect the convection zone flow. Unfortunately, no formalism yet exists by which such a back-reaction might be quantified.

The back-reaction of a fibril field will take a form very different from that of a continuum field. To see this consider their differing reactions to a simple prescribed shear flow $\mathbf{v} = v_0 \sin(ky)\hat{\mathbf{x}}$. A continuum field transverse to this flow has no equilibrium under the ideal induction equation,

$$\mathbf{B} \;=\; B_0\hat{\mathbf{y}} \;+\; B_0 v_0 kt\, \cos(ky)\,\hat{\mathbf{x}} \quad . \tag{1}$$

This field produces an opposing Lorentz force proportional to the growing fluid displacement $F_x \sim -v_x t$; a reaction analogous to an elastic restoring force. It is clear from this fact alone

that even a field which is initially very weak can eventually produce enough back-reaction to stop any flow.

In contrast to a continuum field, a *flux tube* transverse to the flow will reach an equilibrium state. In this equilibrium, magnetic tension force balances the aerodynamic drag from the flow. The unmagnetized medium flows around the flux tube so the Lorentz force does not grow indefinitely. Instead, the flux tube will produce a steady back-reaction opposing the shear flow. When summed over a local ensemble of tubes, this back reaction will constitute a stress on the fluid, and thereby produce an effective viscosity. Furthermore, rather than a simple Newtonian viscosity, the effective back reaction is more accurately described as a viscoelasticity, since cessation of the driving flow $\mathbf{v}$ will not result in the immediate collapse of the shear stress arising from magnetic tension. Instead the stress will relax in a finite time, depending on the flux and drag on the fibrils.

The form of the back-reaction offered by a fibril field can be anticipated by an analogy to the physics of polymer solutions. Fluids permeated with microscopic polymers have been studied by a variety of investigators (Doi and Edwards 1986; Bird *et al.* 1987) over many years. Each polymer strand is buffeted by the thermal fluctuations of the fluid, much as magnetic flux tubes are buffeted by plasma turbulence. The back-reactions of the polymers appear as viscoelastic effects in the dynamics of the fluid. Over short time scales the polymers exert an elastic restoring force, while after longer times the force becomes viscous. Thus a steady shear-flow is possible in a polymer solution. The coefficients dictating this viscoelastic behavior can be derived from the basic physics of the polymers and their coupling to the fluid (Doi and Edwards 1986). In the present work we apply this technique to thin flux tubes permeating a turbulent plasma, in order to derive viscoelastic coefficients describing a fibril field's back-reaction.

Magnetohydrodynamic viscoelastic effects were recently proposed in a model of a magnetized accretion disks (Ogilvie 2001). The proposed model uses a continuum magnetic field, similar to mean-field electrodynamics, from which the back-reaction is the Lorentz force. To recover a viscous regime the author hypothesizes magnetic reconnection with a short relaxation time, similar in effect to a large resistivity. Our approach will be fundamentally different since we assume a fibril field and make no specific assumption about magnetic reconnection.

The next section derives dynamical equations for an isolated magnetic flux tube immersed in a turbulent plasma. The turbulent buffeting drives the flux tube into a statistical equilibrium state in which its magnetic tension is capable of balancing the drag. Section 3 presents the results of nonlinear numerical solutions of the thin flux tube equations under the same conditions. These solutions corroborate the theoretical methods and fix unknown

coefficients. Section 4 derives viscoelastic coefficients for a collection of of individual flux tubes in statistical steady-state. In section 5 we estimate the viscosity for steady state flows in the solar convection zone. Under certain assumptions we find that the flux tubes may produce a viscosity comparable to the well-known turbulent viscosity, which most theoretical models already account for. In the final section we speculate on how the viscoelastic forces may affect flows in the convection zone, including the differential rotation.

2. The Model

2.1. The dynamics of a thin flux tube

Nonlinear, dynamical equations for the evolution of a thin flux tube were proposed by Spruit (1981) and have been refined and extended by subsequent authors (Choudhuri 1990; Cheng 1992; Moreno-Insertis and Emonet 1996). These models are most frequently used to study the buoyant rise of an active region flux tube through the solar convection zone (see e.g. Fisher *et al.* 2000 and references therein.) To simplify our analysis we consider a non-buoyant flux tube immersed in an unstratified turbulent plasma. Without gravitation or rotation the tube experiences only the force of aerodynamic drag, $\mathbf{F}_{\rm d}$, and its own magnetic tension (DeLuca *et al.* 1993). The forces cause an element of tube to accelerate at

$$\frac{d\mathbf{v}}{dt} \;=\; \frac{B^2}{4\pi\rho}\frac{\partial^2\mathbf{r}}{\partial s^2} + \frac{1}{8\pi\rho}\frac{\partial B^2}{\partial s}\,\frac{\partial\mathbf{r}}{\partial s} + \mathbf{a}_{\rm d} \quad , \tag{2}$$

where $B(s)$ is the magnetic field strength and $\mathbf{a}_{\rm d} \equiv \mathbf{F}_{\rm d}/\rho$ is the local acceleration due to drag.

A cylindrical tube segment moving at velocity $\mathbf{v}$, through an external flow with velocity $\mathbf{v}^{(\rm e)}$, feels a drag force per unit volume

$$\mathbf{F}_{\rm d} \;=\; -\,\frac{C_{\rm D}\rho}{\sqrt{\pi\Phi/B}}\,|\mathbf{v}_\perp - \mathbf{v}^{(\rm e)}_\perp|\,(\mathbf{v}_\perp - \mathbf{v}^{(\rm e)}_\perp) \quad , \tag{3}$$

where $\mathbf{v}_\perp$ and $\mathbf{v}^{(\rm e)}_\perp$ are the components of $\mathbf{v}$ and $\mathbf{v}^{(\rm e)}$ perpendicular to the local tangent vector of the tube's axis $\hat{\mathbf{s}} \equiv \partial\mathbf{r}/\partial s$. Although the form of (3) renders the dynamics nonlinear in the general case, a good linear approximation can be made in the case where the time scales of fibril dynamics greatly exceeds those of the turbulence.

The external fluid velocity $\mathbf{v}^{(\rm e)}(\mathbf{x}, t)$ will be replaced here by a random function whose statistics represent those of the turbulence. We will make the approximations that $\mathbf{v}^{(\rm e)}$ is isotropic and has negligibly small correlation time $\tau_{\rm c}$ compared with the dynamical times of

the flux tube (i.e. it is white noise). Under these assumptions the drag term can be replaced by a general expression of the Langevin-type

$$\mathbf{a}_{\rm d} \;\simeq\; \mathbf{f}_\perp(s,t) \;-\; \zeta \mathbf{v}_\perp \quad , \tag{4}$$

where averages over the turbulent fluctuations give $\langle \mathbf{f}_\perp \rangle = 0$ and $\langle \zeta \rangle = \zeta$. The specific drag ζ is found by averaging the definition (4)

$$\zeta \;\equiv\; -\left\langle \frac{\mathbf{a}_{\rm d}\cdot\mathbf{v}_\perp}{|\mathbf{v}_\perp|^2} \right\rangle \;=\; \sqrt{\frac{B}{\pi\Phi}}\, \frac{\langle \mathbf{v}_\perp \cdot (\mathbf{v}_\perp - \mathbf{v}_\perp^{(\rm e)}) |\mathbf{v}_\perp - \mathbf{v}_\perp^{(\rm e)}| \rangle}{|\mathbf{v}_\perp|^2} \quad , \tag{5}$$

where we have taken $C_{\rm D} = 1$, the high-Reynolds number limit (Batchelor 1967).

One limit which can be treated analytically is that of a small tube-velocity, $|\mathbf{v}_\perp^{(\rm e)}| \gg |\mathbf{v}_\perp|$, in which the drag is proportional to the average turbulent velocity and independent of the velocity $\mathbf{v}_\perp$. The expansion of (5) in powers of $|\mathbf{v}_\perp|/|\mathbf{v}_\perp^{(\rm e)}|$ yields two leading order terms whose sum is

$$\zeta \;\simeq\; \frac{3\pi}{8} \sqrt{\frac{B}{\pi\Phi}}\, \langle |\mathbf{v}^{(\rm e)}| \rangle \tag{6}$$

where isotropy has been used to express $\langle |\mathbf{v}_\perp^{(\rm e)}| \rangle = (\pi/4) \langle |\mathbf{v}^{(\rm e)}| \rangle$. In any case, ζ^{-1} is the time-scale on which coherent motions relax by virtue of the random driving.

The general two-point statistics of the stochastic forcing $\mathbf{f}_\perp$ are complicated since they depend on $\mathbf{v}_\perp(s)$ and $\mathbf{v}_\perp(s')$ as well as the tangent vectors $\hat{\mathbf{s}}$ and $\hat{\mathbf{s}}'$. Fortunately we will have need for only the scalar correlation, which we write as

$$\langle \mathbf{f}_\perp(s,t) \cdot \mathbf{f}_\perp(s',t') \rangle \;=\; \Gamma\, C(s-s')\, \tau_{\rm c} \delta(t-t') \quad . \tag{7}$$

We have introduced the correlation function $C(\Delta s)$, which is unity at $\Delta s \equiv s - s' = 0$, and decreases with increasing separation. Its decrease is due to de-correlation of the turbulent velocity at increasing distances, as well as to the differences in perpendicular direction between s and s'. We will assume that $C(\Delta s)$ has a single peak at $\Delta s = 0$ with half width $\sim \ell_{\rm t}$, the turbulent correlation length.

The product $\tau_{\rm c}\delta(t)$ in (7) is a short-hand for the time-correlation of the turbulence. By assumption the turbulence has a very short correlation time, however, the single-time correlation is still finite, and enters appropriately when integrating over the correlation of the noise.

The amplitude factor in expression (7) is set by the single-point, single-time moment

$$\Gamma \;\equiv\; \langle |\mathbf{a}_{\rm d}|^2 \rangle - \zeta^2 |\mathbf{v}_\perp|^2 \;=\; \frac{B}{\pi\Phi} \left[\langle |\mathbf{v}_\perp - \mathbf{v}_\perp^{(\rm e)}|^4 \rangle - \frac{\langle \mathbf{v}_\perp \cdot (\mathbf{v}_\perp - \mathbf{v}_\perp^{(\rm e)}) |\mathbf{v}_\perp - \mathbf{v}_\perp^{(\rm e)}| \rangle^2}{|\mathbf{v}_\perp|^2} \right] \quad , \tag{8}$$

In the small-tube-velocity limit $|\mathbf{v}_\perp| \ll |\mathbf{v}_\perp^{(\mathrm{e})}|$ the factor takes the simple form

$$\Gamma \simeq \frac{8}{15}\frac{B}{\pi\Phi}\langle|\mathbf{v}^{(\mathrm{e})}|^4\rangle \quad , \tag{9}$$

where isotropy has been used to express $\langle|\mathbf{v}_\perp^{(\mathrm{e})}|^4\rangle = (8/15)\langle|\mathbf{v}^{(\mathrm{e})}|^4\rangle$.

The tube's inertia is negligible under many circumstances and the primary dynamics is that of turbulent advection being opposed by magnetic tension. In this situation it is possible to neglect the left hand side of (2). We will define a Lagrangian coordinate s_0 which is the length-coordinate of the material point in some reference configuration. The velocity of the tube may then be written $\mathbf{v} = \partial\mathbf{r}(s_0,t)/\partial t$, and the tube's equation of motion becomes

$$\zeta\left.\frac{\partial\mathbf{r}}{\partial t}\right|_\perp = \frac{B^2}{4\pi\rho}\frac{\partial^2\mathbf{r}}{\partial s^2} + \frac{1}{8\pi\rho}\frac{\partial B^2}{\partial s}\frac{\partial\mathbf{r}}{\partial s} + \mathbf{f}_\perp \quad . \tag{10}$$

2.2. The Mean-Field Theory

Equation (10) describes the dynamics of a thin flux tube buffeted by the turbulent medium in which it is immersed. The random driving $\mathbf{f}_\perp$ will induce random distortions in the axis $\mathbf{r}(s_0,t)$. It is the statistics of these distortions we wish to analyze. We will perform this analysis in the mean-field limit, replacing the randomly fluctuating functions $B(s)$ and $\partial s/\partial s_0$ by their average values. Assuming that the statistics of the axis are homogeneous and isotropic, the mean-field equation reduce to

$$\zeta\frac{\partial\mathbf{r}}{\partial t} = U\frac{\partial^2\mathbf{r}}{\partial s_0^2} + \mathbf{f}_\perp \quad , \tag{11}$$

where the tension coefficient

$$U \equiv \frac{B^2}{4\pi\rho}\left(\frac{\partial s}{\partial s_0}\right)^{-2} \quad , \tag{12}$$

is a constant which, like ζ, depends on the statistical properties of the solution. The right hand side of (11) is now perpendicular to $\hat{\mathbf{s}}$, so the velocity $\mathbf{v}$ will be so automatically.

Equation (11) is that of an elastic string driven by random noise. Models of this type have been studied extensively in the field of polymer physics. Because the equation is linear in the unknown we can propose a Fourier decomposition

$$\mathbf{r}(s_0,t) = \sum_q \mathbf{r}_q(t)\, e^{iqs_0} \quad , \tag{13}$$

and solve immediately for its coefficients

$$\mathbf{r}_q(t) \;=\; \int_{-\infty}^{t} \exp\left[-\frac{Uq^2}{\zeta}(t-t')\right]\,\mathbf{f}_q(t')\,\frac{dt'}{\zeta} \quad . \tag{14}$$

(For simplicity we assume the flux tube is a closed curve and thereby use discrete Fourier transforms.) Thus the distortions of the flux tube depend on the random driving function $\mathbf{f}_\perp$ over all past times.

Under the isotropic mean field approximation the general correlation matrix of the stochastic driving is

$$\langle \mathbf{f}_\perp \mathbf{f}_\perp \rangle \;=\; \tfrac{1}{3}\,\Gamma\, C(s-s')\,\tau_{\rm c}\delta(t-t')\,\mathrm{I} \quad . \tag{15}$$

Introducing the Fourier decomposition of $\mathbf{f}_\perp$ yields mode-correlation statistics

$$\langle \mathbf{f}_q(t)\mathbf{f}^*_{q'}(t')\rangle \;=\; \tfrac{1}{3}\,\Gamma C_q\,\tau_{\rm c}\delta(t-t')\,\delta_{q,q'}\,\mathrm{I} \quad , \tag{16}$$

where C_q is the Fourier transform of the correlation function $C(\Delta s)$. The correlation function itself is defined in terms of extensible coordinates s and s', which are appropriate for describing separations in the turbulent flow. Nevertheless, its Fourier transform is performed with respect to Lagrangian coordinates s_0 and s_0' in which the dynamical solutions are cast. Care must be taken to transform between these coordinates using the mean-field extension factor $\partial s/\partial s_0$.

Forming the general correlation matrix between axis-modes $\mathbf{r}_q$, and using (16) gives

$$\langle \mathbf{r}_q(t)\mathbf{r}^*_{q'}(t')\rangle \;=\; \frac{1}{6}\,\frac{\Gamma C_q \tau_{\rm c}}{\zeta q^2 U}\,\exp\left(-\frac{Uq^2}{\zeta}|t-t'|\right)\,\mathrm{I}\delta_{q,q'} \quad . \tag{17}$$

Axis modes remain correlated over much longer times than the noise that drives them. A mode with wavelength $\lambda = 2\pi(\partial s/\partial s_0)/q$ de-correlates over a time

$$\tau_\lambda \;=\; \frac{\zeta}{Uq^2} \;=\; \frac{\zeta}{4\pi^2 v_{\rm A}^2}\,\lambda^2 \quad . \tag{18}$$

where $v_{\rm A} = B/\sqrt{4\pi\rho}$ is the local Alvén speed.

It is now possible to calculate the coefficients in our mean field equation in terms of the average properties of the axis modes $\mathbf{r}_q$. Tube elements labeled by s_0 and s_0' are separated by a vector

$$\Delta\mathbf{r} \;\equiv\; \mathbf{r}(s_0,t) - \mathbf{r}(s_0',t) \quad . \tag{19}$$

The second moment of this displacement vector is

$$\langle|\Delta\mathbf{r}|^2\rangle \;=\; \frac{4\Gamma\tau_{\rm c}}{\zeta U}\,\sum_q C_q\,\frac{\sin^2(q\Delta s_0/2)}{q^2} \quad , \tag{20}$$

where $\Delta s_0 \equiv s_0 - s_0'$. If the two points are sufficiently separated, $|\Delta s_0| \gg \ell_{\rm t}$, then the sum becomes

$$\sum_q C_q \, \frac{\sin^2(q\Delta s_0/2)}{q^2} \;\simeq\; \tfrac{1}{4}\,\Delta s_0 \int_{-\infty}^{\infty} C(s)\, ds_0 \;\simeq\; \tfrac{1}{2}\,\Delta s_0\, \ell_{\rm t} \left(\frac{\partial s}{\partial s_0}\right)^{-1} \quad , \tag{21}$$

since $C_q \simeq C_0$ over the support of the factor $\sin^2(q\Delta s_0/2)/q^2$ in this limit. The sum of the factor may be relaced by an integral with respect to $dq/\Delta q$, where the spacing bewteen discrete Fourier modes, $\Delta q \ll 1/\Delta s_0$. In this limit, the section of tube between s and s' is a random walk of uncorrelated steps $\ell_{\rm t}$. According to classical theory of random walks, the total number of such steps is $N = \langle|\Delta\mathbf{r}|^2\rangle/\ell_{\rm t}^2$. Thus the total length of the tube-segment is

$$\Delta s \;=\; \langle|\Delta\mathbf{r}|^2\rangle/\ell_{\rm t} \;\simeq\; \frac{2\Gamma\tau_{\rm c}}{\zeta U}\left(\frac{\partial s}{\partial s_0}\right)^{-1} \Delta s_0 \quad . \tag{22}$$

The mean-field extension factor $\partial s/\partial s_0$ can now be equated to the extension $\Delta s/\Delta s_0$ found from the randomly deformed axis. Doing so, and using expression (12) for U yields a relationship

$$\frac{B^2}{4\pi\rho} \;=\; \frac{2\Gamma\tau_{\rm c}}{\zeta} \quad . \tag{23}$$

In the context of the polymer physics of Brownian motion, this expression is a version of the fluctuation-dissipation theorem, linking drag and noise. In the present context, however, it becomes the determining relation for the field strength of the flux tubes at equilibrium.

The right hand side of (23) depends on B through Γ and ζ. Using the small-flux-tube-velocity ($|\mathbf{v}_\perp| \ll |\mathbf{v}_\perp^{(\rm e)}|$) expressions (6) and (9) it is possible to solve explicitly for

$$B \;=\; 3.454 \left(\rho\tau_{\rm c}\,\frac{\langle|\mathbf{v}^{(\rm e)}|^4\rangle}{\langle|\mathbf{v}^{(\rm e)}|\rangle}\right)^{2/3} \Phi^{-1/3} \quad . \tag{24}$$

If we admit tube velocities comparable to the typical turbulent velocity $v_{\rm t}$, then the general expressions for ζ and Γ, i.e. (5) and (8) depend explicitly on B as well as on averages of the relative velocities. If each of the velocity averages scales only as the appropriate power of $v_{\rm t}$, and is independent of B or Φ, then (23) gives the same scaling

$$B \;\simeq\; K'\,(\rho\tau_{\rm c}\, v_{\rm t}^3)^{2/3}\,\Phi^{-1/3} \quad , \tag{25}$$

but with a factor K' that depends on the re-scaled velocity averages.

Expression (25) gives the field strength achieved by the flux tube under the action of turbulence. This represents a statistical equilibrium, where the flux tube's tension is strong

enough to balance the aerodynamic drag of the turbulence. Remarkably, the field strength scales inversely with the tube's flux to the one-third power, so smaller flux tubes will tend to be stronger. This is a natural consequence of the inverse scaling of the drag force with cross-sectional area: thinner tubes couple more effectively to the turbulence, and they must be stronger before their tension can balance the drag force.

DeLuca *et al.* found a scaling similar to (25) for a closed ring of flux immersed in a steady cellular flow pattern (an ABC flow). While the Eulerian correlation time in such a flow is infinite, the tube sees a variation over times $\tau_{\rm c} \sim \ell_{\rm t}/v$ due to its own motion. Using this in expression (25) gives a scaling identical to that found by DeLuca *et al.*.

3. Numerical simulations

To verify the foregoing analysis we perform numerical simulations of flux tube dynamics. The basic thin flux tube model eq. (2), including inertia, is solved subject to the constraint that the magnetic tension coefficient $B^2/4\pi\rho$ is uniform along the tube (*i.e.* that the 2nd term in eq. (2) vanishes); this same constraint follows from the mean field approximation as discussed in §2.2. This constraint also follows if the pressure fluctuations within the tube are assumed to be smoothed out much more quickly than the tube configuration changes, which is expected when $c_{\rm s}/v_{\rm A} \simeq \beta^{1/2} \gg 1$, where c_s is the plasma's sound speed. In the simulations described in this paper, the time scale on which pressure perturbations (sausage waves) within the tube travel a length $\ell_{\rm t}$ is much shorter than the turbulent time scale $\tau_{\rm t}$, so this should be an excellent approximation. The resulting equation involves only inertia, the magnetic tension coefficient, the flux tube curvature vector, and the aerodynamic drag force (eq. 3) due to turbulent motions acting to buffet the tube.

The primary agent driving evolution of the tube is then the external velocity field $\mathbf{v}^{(\rm e)}$ appearing in eq. (3). In our formulation, the average properties of this flow field depend on only two quantities: a characteristic velocity amplitude $v_{\rm t}$ and a characteristic *eddy size* (or correlation length) $\ell_{\rm t}$. An *eddy turnover* time can then defined as $\tau_{\rm t} = \ell_{\rm t}/v_{\rm t}$, which will turn out not to be equivalent to the correlation time of the noise driving the tube. To be consistent with our white-noise assumption we will seek to keep $\tau_{\rm t}$ smaller than all other dynamical scales. At any given time, $\mathbf{v}^{(\rm e)}$ is a function of the Lagrangian arc length s_0, which can be assumed without loss of generality to vary from 0 to 1.

At a fixed time, the velocity at a point $s = s_i = i(\delta s)$ is produced according to the

recipe

$$\mathbf{v}_i^{(\mathrm{e})} = v_\mathrm{t} \sum_{j=1}^{N} \mathbf{w}_j A(\delta s/\ell_\mathrm{t}) \exp\left[-\frac{(i-j)^2(\delta s/N)^2}{2\ell_\mathrm{t}^2}\right], \tag{26}$$

where δs is the arc-length separation between adjacent mesh points ($\delta s \equiv N^{-1}\partial s/\partial s_0$) and $A(\delta s/\ell_\mathrm{t})$ is a normalization factor for the weighting. The velocity is endowed with randomness through an uncorrelated white noise vector $\mathbf{w}_i$. Each 3-vector $\mathbf{w}_i$ is a random variable with unit variance and is completely uncorrelated with any other point: $\langle \mathbf{w}_i \mathbf{w}_j \rangle = \mathrm{I}\delta_{i,j}$. The velocities at points separated by $\Delta s < \ell_\mathrm{t}$ are correlated by virtue of common terms in their respective sums, even though all terms themselves are mutually uncorrelated.

The time correlation of $\mathbf{v}_i^{(\mathrm{e})}$ follows from correlations of the random vectors $\mathbf{w}_i$ which follow from an evolution equation. The vector $\mathbf{w}_i$ is updated in time according to the prescription (Longcope and Fisher 1996)

$$\mathbf{w}_i^{\mathrm{new}} = \exp(-\Delta t/\tau_\mathrm{t})\mathbf{w}_i^{\mathrm{old}} + \sqrt{1-\exp(-2\Delta t/\tau_\mathrm{t})}\mathbf{N}_i, \tag{27}$$

where Δt is the time-step, and $\mathbf{N}_i$ is a freshly generated 3-vector of normal deviates (i.e. zero mean and unit variance). According to this prescription $\mathbf{w}_i$ will become uncorrelated after a time $\sim \tau_\mathrm{t}$.

The numerical methods used to solve eq. (2) are the same as those used to solve for the flux tube evolution described in (DeLuca *et al.* 1993). Briefly, the first and second partial derivatives with respect to Lagrangian arc-length are converted to a centered finite difference form with N uniformly spaced mesh points in s_0. Two additional ghost points are added to each end of the tube with values determined by periodic boundary conditions, since the tube forms a closed ring. The resulting finite difference equations form a set of $6N$ coupled ordinary differential equations which are advanced in time via a standard fourth-order Runge-Kutta technique. These equations result in a solution for the tube node locations and components of velocity normal to the tube's tangent vector.

We perform a set of runs in which Φ, v_t and ℓ_t are varied around nominal values. The nominal values are, initial field strength $B_0 = 10^5\,\mathrm{G}$, correlation length $\ell_\mathrm{t} = 10^9\,\mathrm{cm}$, turbulent velocity $v_\mathrm{t} = 10^4\,\mathrm{cm\,s^{-1}}$, and magnetic flux $\Phi = 10^{18}\,\mathrm{Mx}$. These parameters were chosen to resemble the flux and field strength for a small "elemental" flux tube near the base of the solar convection zone, with values of v_t and ℓ_t corresponding roughly to those from mixing length convection zone parameters. The plasma density in these calculations was assumed to be $\rho = 0.2\mathrm{g\ cm^{-3}}$, which is the value near the base of the convection zone (Böhm-Vitense 1958).

Because we assume the flow inside the tube is incompressible and we ignore sausage waves along the tube, an auxiliary mass conservation equation must also be solved to de-

rive the velocity component parallel to the magnetic tube direction. This is described in (DeLuca *et al.* 1993).

Runs explore variations in Φ, the turbulent velocity $v_{\rm t}$, and the correlation length $\ell_{\rm t}$, while all use the same the initial length, mass density, and initial field strength. All runs start from an initially circular ring with length $L_0 = 2\pi \times 10^{10}$cm, designed to sample a large number (~ 60) of correlation lengths. The Alfvén transit time around the ring, $\tau_A \equiv L/v_{\rm A}$, is an invariant due to incompressibility, and is $\tau_A = 10^6$ seconds for all runs.

A single simulation is run for a period of $6 - 10 \times 10^7$s, or $\sim 60 - 100\ \tau_A$. For the nominal values of $\ell_{\rm t}$ and $v_{\rm t}$ this corresponds to $\sim 600 - 1000\tau_{\rm t}$. The amount of computing resources necessary to carry out these simulations varied widely, ranging from roughly 10 minutes on a laptop computer to over a day on a high performance workstation, depending on the required resolution and the assumed values of $v_{\rm t}$, $\ell_{\rm t}$, or Φ. Resolution varied from 300 mesh points to 2500 mesh points, depending on the values of the above parameters. We encountered some numerical stability problems for high values of $v_{\rm t}$ or low values of $\ell_{\rm t}$.

The numerical simulations form three different series; in each series a single parameter was varied, while all others retained their nominal value. The series explore the effects that changes in Φ, $v_{\rm t}$, and $\ell_{\rm t}$ have on average global properties and on time evolution. In the first series of simulations, the magnetic flux assumed the values $\Phi = 10^{16}$, 10^{17}, 10^{18} and $\Phi = 10^{19}$Mx. In the second series $\ell_{\rm t}$ assumed values of 5×10^8cm, 2×10^9cm, and 4×10^9cm, in addition to its nominal value 1×10^9cm. In the third series $v_{\rm t}$ assumed values of 5×10^3cm s^{-1}, 2×10^4cm s^{-1}, and 4×10^4cm s^{-1}, in addition to the nominal value of 1×10^4cm s^{-1}.

To facilitate discussion of the numerical results, we introduce the abbreviated notation Pii-Ljj-Vkk to refer to a simulation whose values of Φ, $\ell_{\rm t}$, and $v_{\rm t}$, are given by ii $= log_{10}\Phi$, jj $= \ell_{\rm t}/10^8$cm, and kk $= v_{\rm t}/10^3$cm s^{-1}. The simulation with nominal values of all parameters is P18-L10-V10. Table 1 summarizes the parameters of each simulation.

Table 1: Summary of the most important input and derived parameters from the series of flux tube simulations. First 4 rows represent variations in Φ, the next 4 rows show variations in l_t, and the last 4 rows show variations in v_t. The mass density ρ was 0.2 g cm^{-3} for all cases.

Run	[a]N_g	[b]t_{sim} [s]	Φ [Mx]	l_t [cm]	v_t [cm s^{-1}]	[c]$\frac{<L>}{L_0} = \frac{<B>}{B_0}$	[d](var(B))$^{1/2}/B_0$
P16-L10-V10	500	1×10^8	10^{16}	1×10^9	1×10^4	2.36	0.251
P17-L10-V10	400	1×10^8	10^{17}	1×10^9	1×10^4	1.31	0.197
P18-L10-V10	300	1×10^8	10^{18}	1×10^9	1×10^4	0.745	0.111
P19-L10-V10	300	1×10^8	10^{19}	1×10^9	1×10^4	0.395	0.093
P18-L05-V10	1500	6.8×10^7	10^{18}	5×10^8	1×10^4	0.483	0.091
P18-L10-V10	300	1×10^8	10^{18}	1×10^9	1×10^4	0.745	0.111[e]
P18-L20-V10	500	1×10^8	10^{18}	2×10^9	1×10^4	0.883	0.217
P18-L40-V10	500	1×10^8	10^{18}	4×10^9	1×10^4	0.993	0.344
P18-L10-V05	300	1×10^8	10^{18}	1×10^9	5×10^3	0.272	0.093
P18-L10-V10	300	1×10^8	10^{18}	1×10^9	1×10^4	0.745	0.111[e]
P18-L10-V20	500	1×10^8	10^{18}	1×10^9	2×10^4	1.53	0.216
P18-L10-V40	2500	6.2×10^7	10^{18}	1×10^9	4×10^4	3.74	0.377

[a] Number of gridpoints along the tube in the simulation.

[b] Total simulated time.

[c] $< L >$ and $< B >$ represent the value of the loop length and field strength, respectively, averaged over the last half of the simulation. L_0 is the initial loop length, equal to $2\pi \times 10^{10}$ cm in all cases. B_0 is the initial field strength, equal to 10^5 G in all cases.

[d] This column is the square root of the field strength variance about its average value $< B >$ divided by B_0 during the last half of each simulation. This is the rms fluctuation of the field strength about its average value, in units of B_0. It is also the rms fluctuation in L about its average, in units of L_0.

[e] This row is repeated from the 3rd row of this table.

Figure 1 displays a snapshot of a typical configuration at a point of statistical steady-state. This particular case is run P18-L10-V40 at the end of the run, after roughly $60\tau_A$ or $\sim 2400\tau_{\rm t}$ of elapsed time. Generally, flux tube configurations with larger values of Φ or smaller values of $v_{\rm t}$ have a less complex looking configuration than the one shown here.

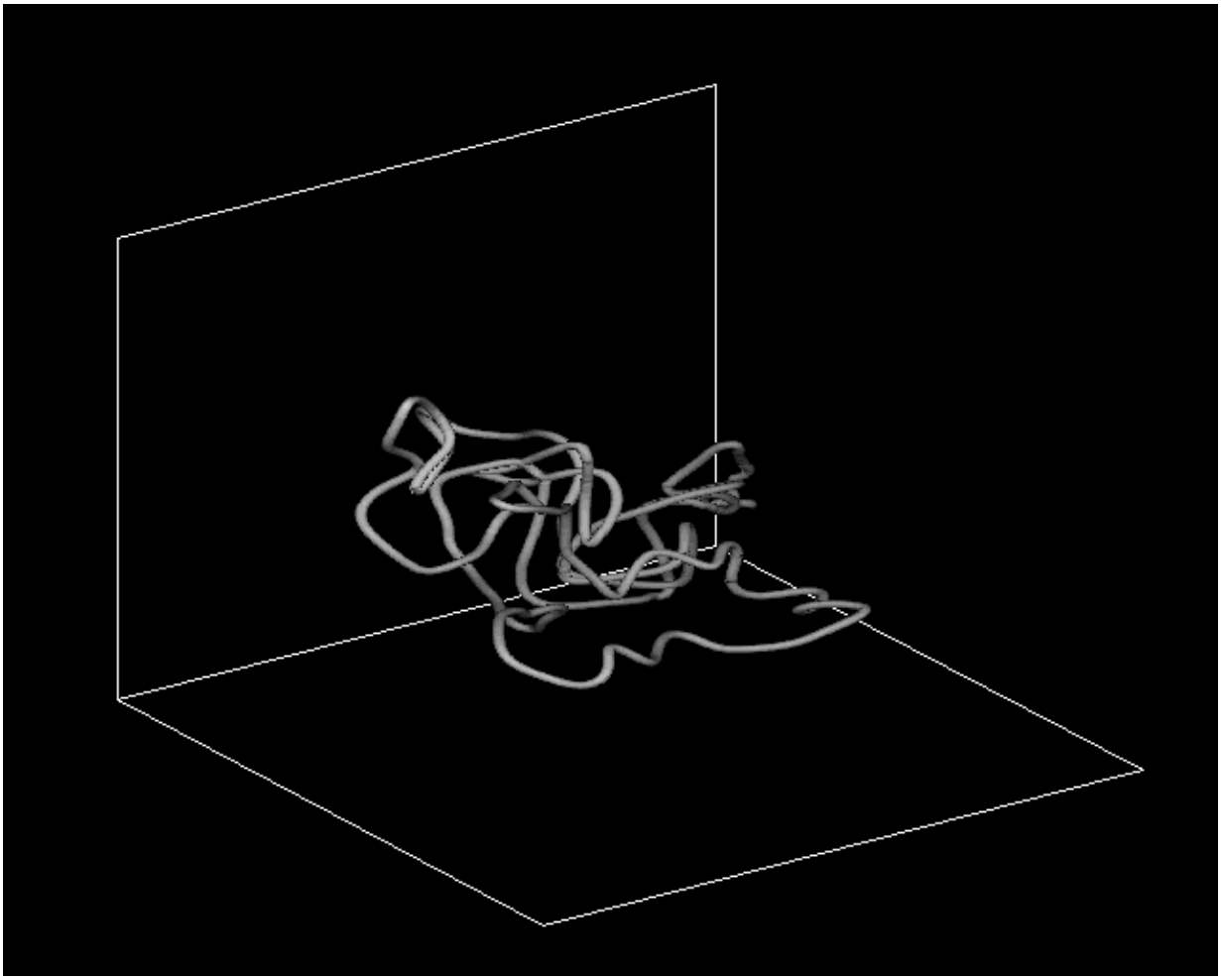

Fig. 1.— A snapshot from run P18-L10-V40.

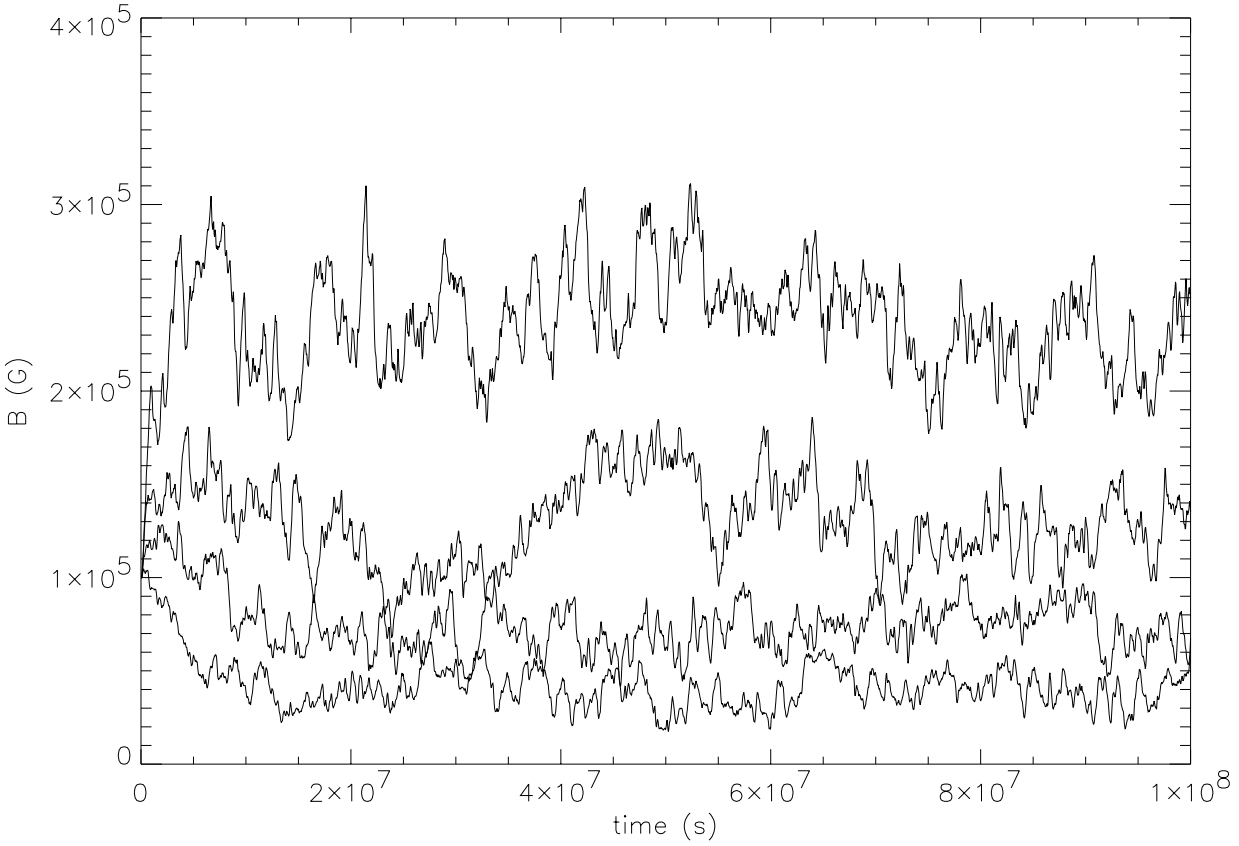

Fig. 2.— The variation of B over time for each of the runs in the Φ-series.

Figure 2 shows the variation of field strength with time for the four values of magnetic flux in the Φ-series. The evolution in all cases shows an initial transient behavior (the "blowup" phase, which can result from either an expansion or contraction from the initial length), followed by attainment of an approximately steady value with random fluctuations about that value. It is interesting to note that a simulation attempted with $\Phi = 10^{20}$ Mx did not result in such a behavior; instead the magnetic tension force overpowered the stochastic driving by the drag force and flux tube collapsed with no statistical steady state being achieved. This "flux ring collapse" behavior was also seen in the simulations of (DeLuca *et al.* 1993). We also find flux ring collapse using nominal values for Φ and $v_{\rm t}$ and $\ell_{\rm t} \sim 2.5 \times 10^8$ cm.

The mean field strength, B, is found by averaging over the last half of each simulation. Figure 3a shows the variation in this average over the Φ-series, P16-L10-V10, P17-L10-V10, P18-L10-V10, and P19-L10-V10; which is well fit by the power law $B \sim \Phi^{-1/4}$. Figure 3b shows the variation over the $v_{\rm t}$-series P18-L10-V05, P18-L10-V10, P18-L10-V20, and P18-L10-V40, The values are well fit by the power law $B \sim v_{\rm t}^{5/4}$. Finally, B varies slightly with $\ell_{\rm t}$ but not enough to yield a convincing power law.

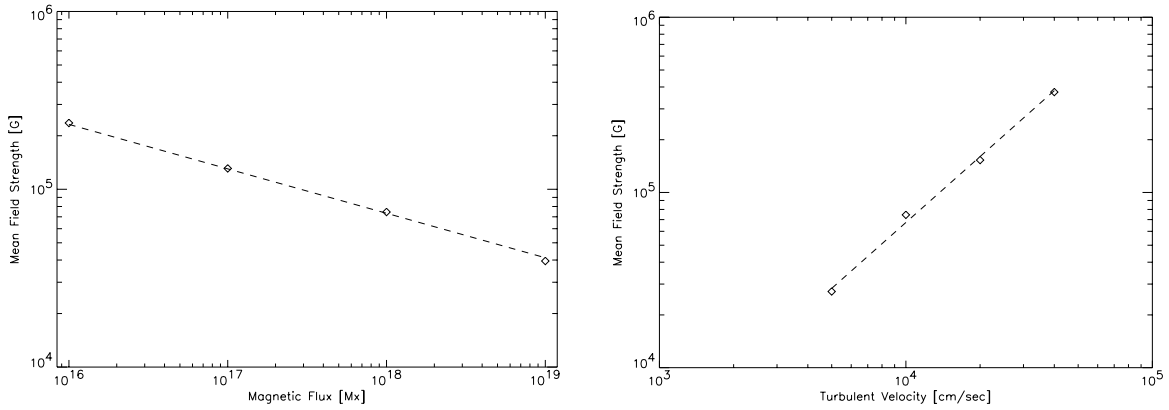

Fig. 3.— Variation in B with Φ (a) and with $v_{\rm t}$ (b). The results of the numerical runs are shown as diamonds. The power law fits are dashed lines.

The numerical simulations reveal that magnetic field strength B scales with magnetic flux Φ and turbulent velocity $v_{\rm t}$. Using density ρ, and turbulent length $\ell_{\rm t}$, to recover the correct dimensions gives a scaling

$$B \;=\; K\,\rho^{5/8}\ell_{\rm t}^{1/2}v_{\rm t}^{5/4}\,\Phi^{-1/4} \quad , \tag{28}$$

where $K \simeq 2.0$.

This empirically derived behavior can be reconciled with the analytic expression (25) if the correlation time of the drag force is the geometric mean between the turbulent correlation time, $\ell_{\rm t}/v_{\rm t}$ and the Alfvén time $\ell_{\rm t}\rho^{1/2}/B$. Substituting this time $\tau_{\rm c} \sim \rho^{1/4}\ell_{\rm t}v_{\rm t}^{-1/2}B^{-1/2}$, into (25) yields the observed scaling (28). The hybrid nature of $\tau_{\rm c}$ might arise from inertia, which was neglected in the analysis of §2, but is included in the numerical simulation. A more detailed analysis, including comparisons of the spatial and temporal spectra $\langle|\mathbf{r}_q|^2\rangle$, would take us too far from our immediate objective of modeling the back-reaction of the tubes. We henceforth adopt (28) as the defining relationship between the turbulence properties and the equilibrium magnetic field strength.

The equipartition field strength, $B_{\rm eq} \equiv \sqrt{4\pi}\rho^{1/2}v_{\rm t}$, is defined to yield an energy density equal to the average kinetic energy density of the turbulence. The equilibrium magnetic field (28) can be written

$$B \;=\; \frac{K}{\sqrt{4\pi}}\,B_{\rm eq}\left(\frac{\Phi}{\Phi_t}\right)^{-1/4} \quad ,$$

where $\Phi_t \equiv \rho^{1/2}\ell_{\rm t}^2 v_{\rm t}$ is the characteristic flux set by the turbulence. Any flux tube with $\Phi < 0.1\Phi_t$ will attain field strength in excess of the equipartition strength as a result of the turbulence. It seems paradoxical, on its face, that turbulence can amplify a magnetic field above the equipartition strength. Upon reflection, however, the aerodynamic drag allows the flux tube to couple to flows outside itself, so local densities are not the appropriate quantities to compare.

4. The Viscoelastic Properties

Up to this point the turbulent fluid has been modeled as a (randomly) prescribed velocity field. This kind of passive driving, where the fluid affects the flux tubes, but is not affected in return, is standard in flux tube models. The Lorentz force is present in the flux tube equation, but it acts only on the fluid within the tube. Here we derive the force exerted by an ensemble of flux tubes upon the unmagnetized fluid.

We will assume that fluid is permeated with magnetic flux tubes, each maintained in statistical steady state by turbulence. The fractional volume occupied by tubes with fluxes

in the range $(\Phi, \Phi+d\Phi)$ will be denoted $f(\Phi)d\Phi$. Due to the assumption of incompressibility, these flux tubes will maintain the same fractional volume even as they evolve, so $f(\Phi)$ will remain constant over time.

All aspects of the back-reaction will depend on the distribution function $f(\Phi)$, about which we can make only a few conjectures. The fraction of volume, or *filling factor*, occupied by all flux tubes is

$$f_\Phi \;=\; \int f(\Phi)\, d\Phi \;\leq\; 1 \quad . \tag{29}$$

In order for the dynamical equations of an isolated tube to apply to each flux tube we should assume that $f_\Phi \ll 1$. The magnetic energy density within a tube is $B^2/8\pi$, where the field strength is maintained by the turbulence at its equilibrium value $B(\Phi)$, given by eq. (28). Thus the magnetic energy density of the entire fibril fields is

$$\epsilon_M \;=\; \frac{1}{8\pi}\int B^2\, f(\Phi)\, d\Phi \;=\; \frac{K^2}{8\pi}\,\rho^{5/4}\ell_{\rm t}v_{\rm t}^{5/2}\,\left\langle \Phi^{-1/2}\right\rangle_\Phi\, f_\Phi \quad , \tag{30}$$

where $\langle\cdot\rangle_\Phi$ is a volume-weighted average over flux tubes only; it is the integral with respect to $f(\Phi)d\Phi/f_\Phi$. Comparing this to the kinetic energy density of the turbulence yields the inverse of the turbulent plasma β

$$\beta_t^{-1} \;\equiv\; \frac{2\epsilon_M}{\rho v_{\rm t}^2} \;=\; \frac{K^2}{4\pi}\Phi_t^{1/2}\left\langle \Phi^{-1/2}\right\rangle_\Phi\, f_\Phi \quad , \tag{31}$$

which is expected to be less than one.

4.1. Shear modulus

The fluid exerts a force on the magnetic flux tube through aerodynamic drag. According to Newton's third law, the flux tube must exert an equal and opposite force back on the fluid. In models with only a single flux tube this back reaction is usually ignored. In a fluid permeated with flux tubes the back reaction must be taken into account. By assumption, the aerodynamic drag in each tube is balanced by magnetic tension. Thus the force felt by the fluid is exactly that of the magnetic tension forces within the collection of flux tubes. The fluid will feel a force equal to the sum of all the tension forces from the ensemble of flux tubes.

The magnetic tension in a thin flux tube is a manifestation of the Lorentz force, which can be written as the divergence of Maxwell stress tensor. The Maxwell stress tensor includes an isotropic piece $-B^2\delta_{ij}/8\pi$ which gives rise to a magnetic pressure gradient. Each flux tube

is assumed to be in pressure balance with the unmagnetized fluid, so the magnetic pressure gradient is always offset by a gradient in plasma pressure. Thus we need only consider the anisotropic part of the remaining piece of the Maxwell stress tensor

$$\mathbf{T} \;=\; \frac{B^2}{4\pi}\,\hat{\mathbf{s}}\,\hat{\mathbf{s}} \quad , \tag{32}$$

where the magnetic field has been taken to be parallel to the tube's axis.

Summing the contributions of all flux tubes within a given element of volume gives a net stress tensor[2]

$$\boldsymbol{\sigma} \;=\; \int \mathbf{T}\, f(\Phi)\, d\Phi \quad = \; 2\epsilon_M \,\left\langle \hat{\mathbf{s}}\,\hat{\mathbf{s}} \right\rangle_{\Phi} \quad , \tag{33}$$

where we have assumed that the directions, $\hat{\mathbf{s}}$, are distributed independently of the fluxes. For an isotropic distribution of $\hat{\mathbf{s}}$ the stress tensor becomes that of a negative pressure $(2/3)\epsilon_M\delta_{ij}$. Evidently the collected tensions of the isotropic ensemble of flux tubes cancels two-thirds of the magnetic pressure. Due to the very high β, it is likely the response to this would be a slight compression of the plasma to compensate.

The plasma pressure cannot compensate any anisotropic contribution to $\boldsymbol{\sigma}$ which may arise due to an anisotropic distribution of $\hat{\mathbf{s}}$. We began by assuming the flux tube was buffeted by isotropic turbulence driving it to an isotropic steady state. If there were a shear flow in addition to the turbulence's, the flux tubes would develop an anisotropy.

Consider the stress at the $z = 0$ plane when the fluid is instantaneously sheared horizontally. Prior to the shearing the flux tubes are in equilibrium with the isotropic turbulence, and so $\hat{\mathbf{s}} = \hat{\mathbf{s}}_0$ is isotropically distributed. An instantaneous shearing, $x \rightarrow x+\gamma z$, will distort all flux tubes. After the shearing the directions will have a additional horizontal component

$$\hat{\mathbf{s}} \;\simeq\; \hat{\mathbf{s}}_0 \;+\; \gamma\hat{\mathbf{x}}(\hat{\mathbf{z}}\cdot\hat{\mathbf{s}}_0) \quad .$$

Averaging a product of these directions, and using the fact that $\hat{\mathbf{s}}_0$ is isotropic, provides an off-diagonal shear stress

$$\boldsymbol{\sigma} \;=\; \tfrac{2}{3}\gamma\epsilon_M\,(\hat{\mathbf{x}}\,\hat{\mathbf{z}} + \hat{\mathbf{z}}\,\hat{\mathbf{x}}) \quad . \tag{34}$$

This stress creates a horizontal force $\boldsymbol{\sigma}\cdot\hat{\mathbf{z}} = 2\hat{\mathbf{x}}\gamma\epsilon_M/3$ on the horizontal plane.

---

[2]This definition is consistent with "stress tensors" in electrodynamics (Jackson 1975), elasticity (Landau and Lifshitz 1986) and Newtonian fluid mechanics (Batchelor 1967) whereby the force density is given by $+\nabla\cdot\boldsymbol{\sigma}$. The force on a volume element includes contributions $\hat{\mathbf{n}}\cdot\boldsymbol{\sigma}$ over its closed surface where $\hat{\mathbf{n}}$ is the *outward normal*. Since hydrodynamic pressure acts inward it will contribute $-p\delta_{ij}$ to σ_{ij}. In a few instances the term "stress tensor" is defined with the opposite sign making it synonymous with the momentum flux tensor Π_{ij} (Bird *et al.* 1987).

Expressing the example above in terms of the symmetric strain tensor $\mathbf{e} = \gamma(\hat{\mathbf{x}}\hat{\mathbf{z}} + \hat{\mathbf{z}}\hat{\mathbf{x}})/2$ gives

$$\boldsymbol{\sigma} \;=\; \tfrac{4}{3}\epsilon_M\,\mathbf{e} \quad . \tag{35}$$

The coefficient in such a stress-strain relation is the *elastic shear modulus* $G = \frac{4}{3}\epsilon_M$. Thus the magnetic flux tubes endow the turbulent fluid with elastic properties, at least on very short times scales.

4.2. Shear viscosity

We summarize here a well-known argument in polymer physics for the emergence of viscoelastic contributions to the bulk viscosity. The instantaneous shear considered above perturbs the isotropic equilibria of the flux tubes. The isotropic turbulence will then buffet the flux tubes causing them to relax back to their isotropic equilibrium distribution and its contribution to the stress will vanish. Each flux tube will relax on a time scale τ_G as each of the Fourier modes in its perturbation relaxes. The stress tensor $\boldsymbol{\sigma}$ will thus decay similarly. To recover a Newtonian viscosity we consider the mean decay time for all modes of the tube.

The limit opposite to the impulsive shear is one in which the fluid is continuously sheared. This will lead to a persistent anisotropy in which the rate of strain $\dot{\mathbf{e}}$ is balanced by the relaxation

$$\langle \hat{\mathbf{s}}\,\hat{\mathbf{s}} \rangle \;=\; \tfrac{1}{3}\,\mathrm{I} \;+\; \tau_G\,\dot{\mathbf{e}} \quad , \tag{36}$$

where the average here is over the axes of a given kind of flux tube. Placing this in (33) and retaining only the anisotropic terms gives a linear relation $\boldsymbol{\sigma} = \mu\dot{\mathbf{e}}$ where the coefficient

$$\mu \;=\; \frac{1}{4\pi}\int f(\Phi) B^2\,\tau_G\,d\Phi \quad , \tag{37}$$

is the *dynamic shear viscosity*.[3]

The time scale τ_G describes the relaxation of a given flux tube to its statistical equilibrium. This will depend on how the flux tubes within the tangle interact with one another. The dynamical interaction between high-β flux tubes, including full and partial reconnection, is still being actively studied (Linton *et al.* 2001) and can not yet be easily incorporated into a model like ours. Nevertheless, it is possible to proceed under two different assumptions,

[3]It is customary in MHD to denote the dynamic shear viscosity by μ in order to reserve η for the magnetic diffusivity. We follow this custom here even though we will always assume a perfectly conducting plasma. Nor will this cause confusion with the elastic shear modulus, which we denote G.

which conceptually bracket all foreseeable cases. The *Rouse limit* obtains when flux tubes can reconnect so readily that they pass through one another effortlessly. The *entangled limit* obtains when flux tubes can never reconnect and bounce off each other instead. We expect the viscoelastic parameters found in these two limiting cases to bound those in cases where flux tubes reconnect in more complicated ways.

4.2.1. The Rouse model

Since flux tubes in the Rouse limit do not interact with one another, each obeys the dynamical equations of a single tube. An impulsive shear introduces perturbations $\mathbf{r}_q$ at all wavelengths up to one extending over the tube's entire length $\lambda = L$. A mode of wave-length λ will relax over a time τ_λ given by eq. (18). We will define this $\tau_\lambda = \tau_L(q_L/q)^2$ where the wave-number $q = (\partial s/\partial s_0)2\pi/\lambda$, q_L is the wave-number for a mode covering the whole tube and τ_L is its relaxation time. The net effect of the dynamics of all these modes on the effective time-dependent decay of the shear modulus takes the form

$$G(t) \;=\; G(0)\,\frac{q_L}{q_t}\,\sum_{p=1}^{q_t/q_L}\exp\left[-\frac{2t}{\tau_L/p^2}\right] \quad , \tag{38}$$

where q_t is the wavenumber corresponding the $\ell_{\rm t}$, the smallest perturbation. The relaxation time for the entire tube is that which characterizes the decay of the shear modulus (Doi and Edwards 1986)

$$\tau_G \;=\; \int_0^\infty \frac{G(t)}{G(0)}\,dt \;\simeq\; \frac{\ell_{\rm t}}{L}\,\frac{\tau_L}{2}\sum_{p=1}^{\infty}\frac{1}{p^2} \;=\; \frac{\zeta L\ell_{\rm t}}{48v_{\rm A}^2} \quad , \tag{39}$$

using (18) for $\tau_L = \tau_\lambda(L)$. This quantity depends on total flux Φ as well as on the total length of the tube L.

For concreteness we will take our flux tubes to be a set of closed curves with a distribution of total lengths L. The total length is not a constant of the motion for a thin flux tube, but under the assumption of incompressibility, the total volume V is. Thus our population of flux tubes will be described by their distribution of fluxes Φ and volumes V.

A more convenient constant of the motion to describe the flux tube population is the volume per flux

$$\Upsilon \;\equiv\; \frac{V}{\Phi} \;=\; \frac{L}{B} \quad . \tag{40}$$

The distribution of flux tubes may have arisen through processes of fragmentation, self-reconnection, and their inverses (see fig. 4). None of these processes is described by eq. (2),

nor do they preserve flux or volume. A closed tube fragments when its cross section breaks into two pieces, giving rise to two closed flux rings of equal length. The resulting tubes have fluxes which sum to the flux of the original tube, but Υ in each tube is the same as in the original; Υ is preserved by fragmentation. A closed tube can break into two shorter tubes by crossing itself and reconnecting at the crossing point. The Υ values of the resulting tubes sum to that of the original, but the flux Φ is preserved in each piece. After many fragmentations, self-reconnections and inverses the set of tubes will have a distribution of Φ and Υ values. If the rates of the individual processes were independent of the conserved quantity, then Φ and Υ would be uncorrelated, and the fractional volume would be a product

$$f(\Phi, \Upsilon) \;=\; f(\Phi)\, p(\Upsilon) \quad , \tag{41}$$

where $f(\Phi)$ is as before and $p(\Upsilon)$ is the distribution of volume-per-mass among individual flux tubes.

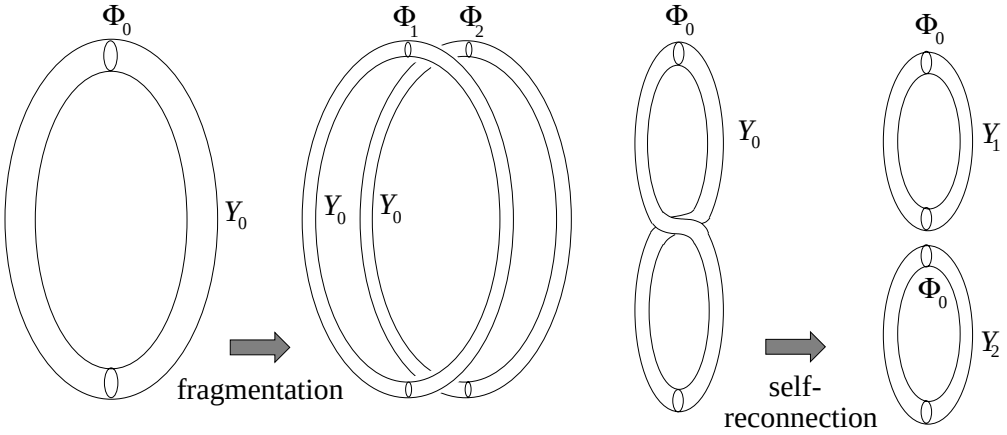

Fig. 4.— The processes of fragmentation and self-reconnection by which a single closed flux tube may break into two. Under fragmentation (left) a tube of flux Φ_0 breaks into tubes with $\Phi_1 + \Phi_2 = \Phi_0$, and the volume per flux Υ_0 is preserved. Under self-reconnection (right) a tube with volume-per-flux Υ_0 breaks into tubes such that $\Upsilon_1 + \Upsilon_2 = \Upsilon_0$, and the flux Φ_0 is preserved.

Using the relaxation time (39), expression (37), and averaging over both Φ and Υ yields a viscosity

$$\mu_R \;=\; \frac{K^{3/2}\sqrt{\pi}}{128}\,\rho^{3/2} v_{\rm t}^2 \Phi_t^{7/8} f_\Phi \left\langle \Upsilon \right\rangle_\Phi \left\langle \Phi^{-7/8} \right\rangle_\Phi \quad , \tag{42}$$

where the equilibrium magnetic field strength, eq. (28), has been used. In order to obtain quantitative estimates we use the small-velocity limit of ζ, eq. (6), here and in later expression. It is not clear that this approximation describes every Fourier mode in a general flux tube, but the full set of numerical simulations required to derive the scaling of ζ is beyond the scope of this paper. The small-velocity limit does apply to the longest wave-lengths of a tube and we thus will adopt it to facilitate the calculation of viscoelastic properties.

When a shear flow is initiated the strain $\mathbf{e}$ will increase linearly in time. As it does the elastic stress $G\mathbf{e}$ increases as well. After a time

$$\bar{\tau}_{\rm r} \;=\; \frac{\mu_R}{G} \;=\; \frac{3\pi^{3/2}}{64K^{1/2}}\,\Phi_t^{3/8}\,\frac{\left\langle \Phi^{-7/8} \right\rangle_\Phi}{\left\langle \Phi^{-1/2} \right\rangle_\Phi} \rho^{1/2}\,\left\langle \Upsilon \right\rangle_\Phi \quad , \tag{43}$$

the stress will approach the viscous stress, to which it will ultimately asymptote. This is the average relaxation rate for all of the flux tubes. If the distribution contains an accumulation of vanishingly small flux tubes so that $\left\langle \Phi^{-7/8} \right\rangle_\Phi$ diverges, then this asymptote will never occur. Smaller flux tubes have greater aerodynamic drag and couple more effectively to the fluid, and it appears that when their density is sufficiently great this strong coupling prevents the kind of yielding that typifies individual thin flux tubes. This state of affairs is similar to the case of continuum MHD which contains a purely elastic back-reaction force in the form of the Lorentz force. Moreover, an infinite relaxation time $\bar{\tau}_R$ implies that the stress tensor increases without bound and any flow will eventually be quenched by the elastic stresses of the flux tubes. Conversely, when there are few enough of these arbitrarily small flux tubes that $\left\langle \Phi^{-7/8} \right\rangle_\Phi$ remains bounded then the stress will cease its elastic growth after finite time $\sim \bar{\tau}_{\rm r}$.

4.2.2. The entangled model

Opposite to the Rouse limit, where flux tubes can pass effortlessly through one another, is the entangled limit, where the flux tubes form mutually impenetrable barriers. The resulting gas of entangled, flexible chains is far more difficult to analyze than the non-interacting Rouse system. A single flux tube finds itself confined within an ever-evolving tangled mesh composed of all other tubes. The starting point for analysis is the length-density

$$\rho_L \;=\; \int f(\Phi)\frac{B}{\Phi}\,d\Phi \;=\; \frac{K f_\Phi}{\ell_{\rm t}^2}\,\frac{\left\langle \Phi^{-5/4} \right\rangle_\Phi}{\Phi_t^{-5/4}} \quad , \tag{44}$$

characterizing the ensemble of tubes. The length-density is the length of tubes (regardless of flux) per unit volume of permeated fluid. A plane-segment of area A will be pierced an average of $A\rho_L$ times by tubes of different fluxes.

The tubes offer severe mutual constraints on dynamics, termed "entanglements" in polymer physics. Of significance for this work, the presence of the entanglement constraints greatly increase relaxation times and thus the effective fluid viscosity. Tubes undergoing interacting (entangled) dynamics will endow the fluid with higher viscosity than tubes with an identical distribution of Φ and Υ undergoing non-interacting (Rouse) dynamics.

Surprisingly the presence of these topological entanglement constraints introduces a new length scale called the entanglement length, $\ell_{\rm e}$. Tube segments smaller than $\ell_{\rm e}$ will be almost unaffected by the entanglement constraints, while longer segments experience strong constraints on their dynamics. The entanglement length scale is much longer than the typical distance between tubes, because the motion of a "test tube" must couple to several others in order to "feel" a strong topological constraint. Therefore, even in a dense melt of entangled polymer chains, segments that just span a single entanglement length $\ell_{\rm e}$ can consist of up to 10^2 monomer units.

In spite of its importance, a quantitative theory for the entanglement length ℓ_e is still an unsolved problem in polymer physics. Recent contributions of scaling theory (Colby and Rubinstein 1990), simulations (Everaers 1998) and careful empirical deductions from systematic data (Fetters *et al.* 1999) have led to the following current view. (i) When the chains are dense, the entanglement length is a near universal $O(10)$ multiple of the "packing length" of the monomer units (in our case this is the turbulent correlation length $\ell_{\rm t}$). (ii) When the chains are not dense, the entanglement length scales as a power of the length-density $\ell_{\rm e} \sim (\rho_L \ell_{\rm t}^2)^{-\alpha}$ with the exponent α taking values close to one, depending on the exact physics of the interactions (candidate models have suggested values of exactly 1 and 4/3 [McLeish 2002]). Combining these two criteria provides estimate of the entanglement length for our problem,

$$\ell_{\rm e} \;\simeq\; 10\ell_{\rm t}^{-5/3}\rho_L^{-4/3} \;=\; 10K^{-4/3}\,\ell_{\rm t}\,f_\Phi^{-4/3}\,\Phi_t^{-5/3}\left\langle\Phi^{-5/4}\right\rangle_\Phi^{-4/3} \quad . \tag{45}$$

Since the total filling factor $f_\Phi \ll 1$, the entanglement length will be many times $\ell_{\rm t}$.

At present, the most successful model for entangled dynamics considers the set of entanglements to form a constraining "tunnel"[4] of radius $\ell_{\rm e}$ about each flexible chain. This forces it into curvilinear motions along the constraining tunnel at scales of ℓ_e and longer.

[4]The polymer physics literature invariably uses the term "tube" here. We have chosen to substitute the term "tunnel" since our fundamental chain is also called a "tube" (i.e. of flux).

The resulting dynamics is characterized by a relaxation time of the full chain which scales a power of ℓ_e

$$\tau_r^{(\mathrm{e})}(L) \;\simeq\; \tau_R(\ell_\mathrm{e}) \left(\frac{L}{\ell_\mathrm{e}}\right)^{\xi} \;=\; \tau_R(L) \left(\frac{L}{\ell_\mathrm{e}}\right)^{\xi-2} \quad . \tag{46}$$

Since the constrained relaxation cannot proceed faster than the unconstrained (Rouse model) relaxation we see from the final expression that $\xi \geq 2$.

One well-studied example of constrained motion is the simple curvilinear diffusion, termed "reptation" (Doi and Edwards 1986), of linear chains (i.e. chains with two free ends) for which $\xi > 3$ (Doi and Edwards 1986). It is not clear whether magnetic flux tubes are better modeled as linear chains (with free ends) or as closed *rings*. There has been a considerable, although more restricted, investigation in the polymer physics literature into the dynamics of entangled ring polymers experimentally (Roovers 1988) and theoretically (Rubinstein 1986; Obhukov *et al.* 1994; Brown *et al.* 2001). If the rings are not mutually interlinked then, in the presence of an effective *network* of permanent constraints, they are thought to form self-similar structures known from percolation theory as "lattice animals" (Cates and Deutsch 1986). These have the property that their radius of gyration $R_g \sim L^{1/4}$ rather than $L^{1/2}$ for linear chains. The diffusion of loops at all length-scales around the entangled rings endows the terminal relaxation time with a scaling intermediate between that of unentangled chains and entangled linear chains, so $2 < \xi < 3$ in expression (46).

The behavior of rings in a melt of other rings is considerably more complex, as it involves a strong contribution of cooperative effects from the finite lifetime of the entanglement constraints. The scaling of the effective viscosity with flux tube length L, however, is certainly bounded below by the unentangled Rouse case, and above by the entangled linear polymer case. A single flux tube of length L will then contribute to the viscosity

$$\mu_e(L) \;=\; \mu_R(\ell_e) \left(\frac{L}{\ell_\mathrm{e}}\right)^{\xi} \quad , \tag{47}$$

where $\mu_R(\ell_\mathrm{e}) \equiv B^2 \tau_G(\ell_\mathrm{e})/4\pi$ is the integrand of (37) with L replaced by ℓ_e. Guided by the results from polymer physics we will hereafter adopt the value $\xi = 5/2$ appropriate for an ensemble of closed rings.

Summing up the contributions (47) over the entire distribution of lengths, $L = B\Upsilon$, yields a Newtonian viscosity

$$\begin{aligned} \mu_e &= \frac{\sqrt{\pi}\rho v_\mathrm{t} \ell_\mathrm{t} \ell_\mathrm{e}^{-3/2}}{128} \int f(\Phi,\Upsilon)\, B^3 \Upsilon^{5/2} \Phi^{-1/2}\, d\Phi\, d\Upsilon \\ &= \frac{K^5\sqrt{\pi}}{1280\sqrt{10}}\, \rho^{9/4} \ell_\mathrm{t}^{-3/2} v_\mathrm{t}^{7/2}\, f_\Phi^3\, \Phi_t^{15/4} \left\langle \Phi^{-5/4} \right\rangle_\Phi^3 \left\langle \Upsilon^{5/2} \right\rangle_\Phi \quad , \end{aligned} \tag{48}$$

using the small-velocity limit eq. (6) for ζ, and expression (45) for the entanglement length $\ell_{\rm e}$. It is noteworthy that the viscosity can diverge in the entangled limit even if it would not in the Rouse limit, since it is possible for $\left\langle \Phi^{-7/8} \right\rangle_\Phi$ to be bounded while $\left\langle \Phi^{-5/4} \right\rangle_\Phi$ is not. As predicted the entangled viscosity grows much faster with filling factor than does the Rouse limit: $\sim f_\Phi^3$ rather than $\sim f_\Phi$.

5. Viscoelasticity of the solar convection zone

The foregoing presented a general formalism for the dynamics of a turbulent fluid permeated with flux tubes. It assumed that each flux tube was in statistical equilibrium with homogeneous, isotropic turbulence characterized by length-scale $\ell_{\rm t}$ and velocity $v_{\rm t}$. The back-reaction of the entire collection of flux tubes took the form of a viscoelastic response characterized by an elastic shear modulus G and a dynamic shear viscosity μ. These quantities depended on the turbulent fluid through $\ell_{\rm t}$, $v_{\rm t}$ and ρ, and on the properties of the flux tube distribution.

In order to estimate the possible significance of flux tubes on the structure of the solar convection zone (CZ) we will compare their viscosity to the traditional turbulent viscosity $\mu_t \equiv \rho v_{\rm t} \ell_{\rm t}$. Each viscosity will depend on the local turbulence at a given depth, as modeled by mixing length theory (Böhm-Vitense 1958). We take the local values of $\ell_{\rm t}$ and $v_{\rm t}$ from the mixing length model and apply these to the homogeneous, isotropic calculation at that depth. Figure 5 shows the variation of the mixing length $\ell_{\rm t}$ along with the quantities $\Phi_t \equiv \rho^{1/2} \ell_{\rm t}^2 v_{\rm t}$ and $B_{\rm eq} = \sqrt{4\pi} \rho^{1/2} v_{\rm t}$ over the convection zone using the CZ model of Spruit (1974).

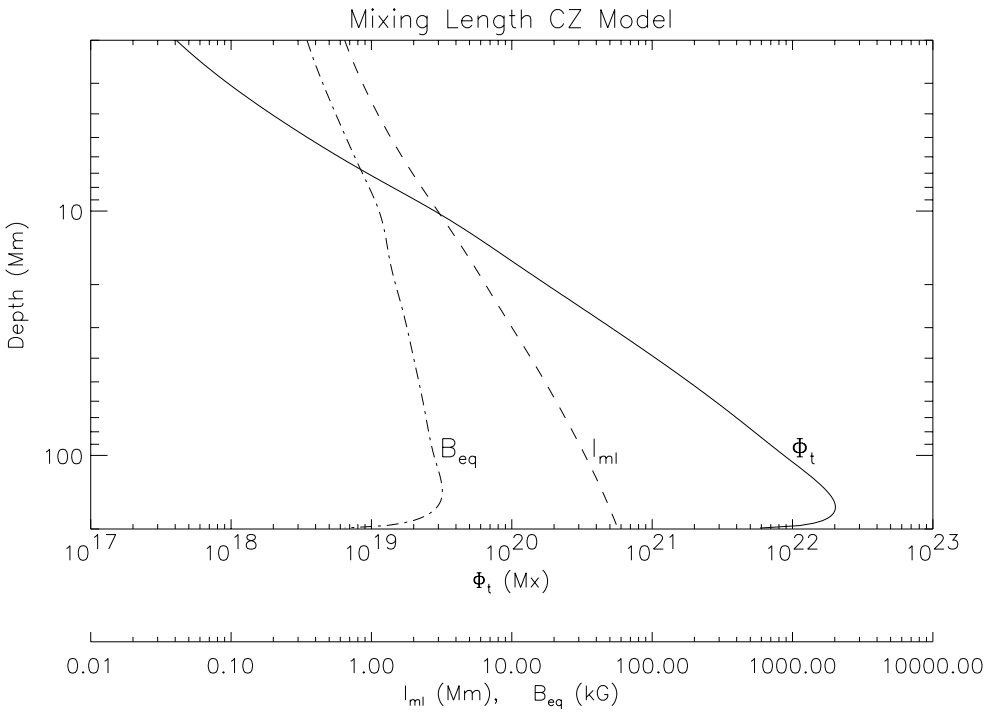

Fig. 5.— The mixing length $\ell_{\rm t}$ and the quantities Φ_t and $B_{\rm eq}$ plotted against the depth running vertically downward.

Viscoelastic properties also depend on the distribution of fluxes and volumes of the flux tubes, about which very little is known. It might be possible to infer the flux distribution from photospheric observation. Deep magnetograms of the quiet Sun show surface flux distributions $N(\Phi) \sim \exp(-\Phi/\bar{\Phi})$, where $\bar{\Phi} \simeq 3 \times 10^{18}$ Mx (Schrijver *et al.* 1997). Exponential distributions of this form can be explained theoretically as the result of continued fragmentation, merging and emergence of flux tubes (Schrijver *et al.* 1997). Any plane passing through the hypothetical isotropic, homogeneous flux tube distribution would be pierced by tubes in the range $(\Phi, \Phi + d\Phi)$ with a density

$$N(\Phi)\, d\Phi \;=\; \frac{B}{\Phi}\, f(\Phi)\, d\Phi \;\sim\; \Phi^{-5/4}\, f(\Phi)\, d\Phi \quad , \tag{49}$$

after using eq. (28) for $B(\Phi) \sim \Phi^{-1/4}$. Regarding the quiet Sun photosphere to be just such a sampling plane implies that $f(\Phi) \sim \Phi^{5/4} \exp(-\Phi/\bar{\Phi})$.

Moments of the exponential distribution above all scale with the mean flux $\bar{\Phi}$

$$\langle \Phi^p \rangle_\Phi \;=\; \frac{\Gamma(p + \frac{9}{4})}{\Gamma(\frac{9}{4})}\, \bar{\Phi}^p \quad , \tag{50}$$

as long as $p > -9/4$. Other well-behaved distributions $f(\Phi)$ will have similar scalings, but with different constants. For concreteness we will adopt the exponential form where $\bar{\Phi}$ depends on depth, achieving its observed value $\bar{\Phi} = 3 \times 10^{18}$ Mx at the solar surface.

The average of the flux distribution, $\bar{\Phi}$, is expected to vary with depth, perhaps in a fashion similar to the characteristic flux Φ_t shown in fig. 5. At the solar surface, where $\bar{\Phi}$ is actually observed, $\Phi_t \simeq 4 \times 10^{17}$ Mx, so $\bar{\Phi}/\Phi_t \sim 10$. Flux tubes at the very base of the CZ are believed to be the source of bipolar active regions. If observed active regions form a representative sampling of this population then we expect $\bar{\Phi} \sim \Phi_t \sim 10^{22}$ Mx. It is entirely possible, even very likely, that only the large end of the population satisfy the requirements for emergence so $\bar{\Phi}/\Phi_t < 1$ at the base of the CZ.

The volumetric filling factor of the flux tubes in the solar convection zone, f_Φ, is difficult to estimate since its definition depends on the assumed dichotomy between field-free plasma and flux tubes. We will use expression (31) to replace f_Φ with values of the turbulent β, which has been estimated to be a few percent (Parker 1984).

Of all the properties of the flux tube mixture, the distribution of volume to flux, Υ, is least related to observable quantities. To cast estimates in more intuitive terms we will work in terms of the average of flux tube lengths

$$\langle L \rangle_\Phi \;=\; K \rho^{1/2} v_{\rm t}\, \Phi_t^{1/4} \left\langle \Phi^{-1/4} \right\rangle_\Phi \langle \Upsilon \rangle_\Phi \quad , \tag{51}$$

found by performing the same flux-tube-only average to both side of the expression $L = \Upsilon B$, and asuming that Φ and Υ are independently distributed, as we argued previously they might be.

The largest flux tubes will be those toroidal tubes, found at the base of the CZ, whose emergence produces active regions. According to the Babcock dynamo picture these tubes will be wound up by differential rotation, achieving a total length of ten circumferences after one solar cycle. Using the mixing length, $\ell_{\rm t} = 60$ Mm, at the base of the CZ, gives $\langle L \rangle_\Phi \sim 500 \ell_{\rm t}$. Much less is known about the lengths of flux tubes in the middle or top of the CZ, so this is the best estimate we can offer. A flux tube must span several eddies in order to be maintained by turbulence against tension-induced self-collapse. Thus no single flux tube in the distribution can be shorter than $\sim 10\ell_{\rm t}$ (having a diameter of $3\ell_{\rm t}$) and the average of *all* tubes could not be much smaller than twice this minimum $\langle L \rangle_\Phi \sim 20\ell_{\rm t}$.

In the Rouse limit the effective viscosity is given by expression (42). Dividing this by the local turbulent viscosity and making the substitutions described above gives

$$\frac{\mu_R}{\mu_t} \;=\; \frac{\pi^{3/2}}{32K^{3/2}} \frac{\Phi_t^{1/8} \left\langle \Phi^{-7/8} \right\rangle_\Phi}{\left\langle \Phi^{-1/2} \right\rangle_\Phi \left\langle \Phi^{-1/4} \right\rangle_\Phi} \frac{\langle L \rangle_\Phi}{\ell_{\rm t}} \, \beta_t^{-1} \;\simeq\; 0.067 \left(\frac{\bar{\Phi}}{\Phi_t} \right)^{-1/8} \frac{\langle L \rangle_\Phi}{\ell_{\rm t}} \, \beta_t^{-1} \quad , \qquad (52)$$

using $K = 2.0$ found in the simulations. This shows that the effectiveness of the flux tubes in redistributing momentum depends on their length, but very little on their fluxes. Adopting the values $\beta_t^{-1} = 0.03$ and $\langle L \rangle_\Phi / \ell_{\rm t} = 500$, discussed above gives $\mu_R \simeq \mu_t$. This demonstrates that even tubes which do not interact with one another (i.e. the Rouse model) can endow the fluid with an additional viscosity of the same magnitude as the turbulent viscosity. The effectiveness of flux tubes depends on their average lenght; a distribution of the shortest plausible flux tubes, $\langle L \rangle_\Phi \sim 20\ell_{\rm t}$, would create a viscosity only 4% of the turbulent viscosity, and their effectiveness would increase above this minimum value.

The entangled limit obtains when flux tubes are mutually impenetrable and extend over distances much greater than the entanglement length $\ell_{\rm e}$. The ratio of the average tube to the entanglement length, (45), is

$$\frac{\langle L \rangle_\Phi}{\ell_{\rm e}} \;\simeq\; \frac{(4\pi)^{4/3}}{10K^{4/3}} \frac{\Phi_t \left\langle \Phi^{-5/4} \right\rangle_\Phi^{4/3}}{\left\langle \Phi^{-1/2} \right\rangle_\Phi^{4/3}} \frac{\langle L \rangle_\Phi}{\ell_{\rm t}} \, \beta_t^{-4/3} \;=\; 1.3 \left(\frac{\bar{\Phi}}{\Phi_t} \right) \frac{\langle L \rangle_\Phi}{\ell_{\rm t}} \, \beta_t^{-4/3} \quad , \qquad (53)$$

For values $\beta_t^{-1} = 0.03$, $\bar{\Phi} = \Phi_t$ and $\langle L \rangle_\Phi / \ell_{\rm t} = 500$ this ratio will be 6, on the verge of being much greater than unity. Thus we expect flux tubes at the base of the CZ to exist just within the entangled limit. In the lower limit, however, $\langle L \rangle_\Phi \sim 20\ell_{\rm t}$, the tubes are safely out of the entangled limit and the Rouse-limit viscosity (52) clearly applies to such a short distributions.

In the entangled limit, the flux tubes collide with one another permitting a more effective redistribution of momentum. The importance of interaction means that the effective viscosity scales as a higher power of the filling factor, and thus a higher power of β_t^{-1}. The ratio of viscosities is

$$\frac{\mu_e}{\mu_t} = \frac{\pi^{7/2}}{\sqrt{4000}K^{7/2}} \frac{\Phi_t^{13/8} \left\langle \Phi^{-5/4} \right\rangle_\Phi^3}{\left\langle \Phi^{-5/8} \right\rangle_\Phi \left\langle \Phi^{-1/2} \right\rangle_\Phi^3} \frac{\left\langle L^{5/2} \right\rangle_\Phi}{\ell_{\rm t}^{5/2}} \beta_t^{-3} = 0.125 \left(\frac{\bar{\Phi}}{\Phi_t} \right)^{-13/8} \frac{\left\langle L^{5/2} \right\rangle_\Phi}{\ell_{\rm t}^{5/2}} \beta_t^{-3} \quad (54)$$

Like the Rouse-limit viscosity, this expression scales with tube lengths and inversely with turbulent β, but also depends significantly on the average flux, $\bar{\Phi}$. The values used above yields a viscosity far greater than the turbulent value $\mu_e \simeq 19\mu_t$.

If the addition of such a substantial viscosity could quench the dynamo action, then we might argue that the mean field strength will be limited to that value at which $\mu_e \simeq \mu_t$. Inverting eq. (54) gives the restriction

$$\beta_t^{-1} \leq \frac{K^{7/6} 4000^{1/6}}{\pi^{7/6}} \frac{\left\langle \Phi^{-5/8} \right\rangle_\Phi^{1/3} \left\langle \Phi^{-1/2} \right\rangle_\Phi}{\Phi_t^{13/24} \left\langle \Phi^{-5/4} \right\rangle_\Phi} \frac{\ell_{\rm t}^{5/6}}{\left\langle L^{5/2} \right\rangle_\Phi^{1/3}}, = 2.0 \left(\frac{\bar{\Phi}}{\Phi_t} \right)^{13/24} \frac{\ell_{\rm t}^{5/6}}{\left\langle L^{5/2} \right\rangle_\Phi^{1/3}} \quad . \quad (55)$$

Taking $\bar{\Phi} = \Phi_t$ and $\left\langle L^{5/2} \right\rangle_\Phi^{1/3} = (500\ell_{\rm t})^{5/6}$ gives a maximum value for the inverse turbulent β of $\beta_t^{-1} = 0.013$.

6. Discussion

We have formulated a theory for a turbulent fluid permeated with fibril magnetic fields. The back-reaction of the fields upon the turbulence will be a viscoelastic one. Over short time scales the field will resist deformation elastically, just as it does in conventional MHD. Unlike a conventional magneto-fluid, a fibril field is not "frozen" to the fluid it permeates and will permit steady flow across its mean direction. The coupling between the fluid and the field provides an effective viscosity.

To demonstrate this claim we developed a model of a collection of flux tubes embedded in homogeneous, isotropic turbulence. The turbulence drives each flux tube toward an equilibrium magnetic field strength at which its tension can, on average, balance the aerodynamic drag. Numerical simulations verify this fact, and show how the equilibrium field strength scales with the tube's flux, and the properties of the turbulence. In equilibrium, the fibril field will react with an elastic modulus proportional to its energy density.

The effective viscosity of the fibril field depends on the rate at which the mesh of flux tubes relaxes back to its statistical equilibrium. If the mesh is even moderately dense, this

relaxation process will involve interaction among the tubes. Thus the effective viscosity depends on how colliding tubes interact. We considered two extreme cases, which conceptually bracket any realistic interaction physics: non-interacting tubes (the Rouse limit) or impenetrable tubes (the entangled limit). Modeling the convection zone turbulence with the mixing length model we found that the non-interacting limit (Rouse) produced a viscosity roughly equal to that due to turbulence. The most restrictive interactions possible (entangled) produce significant viscosity even when the magnetic field has one percent of the energy. This viscosity may well be one of the factors which limits the strength of dynamo-produced magnetic fields.

Much more study will be necessary before we can say with any confidence how the Sun's fibril field affects the circulation in the solar convection zone. Our preliminary results do, however, hold promise for some of the area's more important questions. For example, observational evidence suggests that magnetic field strengths in active region flux tubes *exceed* that of equipartition with the turbulent energy density. This observation is at odds with continuum MHD models which face "dynamo quenching" for $\beta_t^{-1} \gtrsim Rm^{-1/2} \sim 10^{-6}$ (Vainshtein and Cattaneo 1992). Our results show that viscoelastic response will affect the flow only for much larger energy densities of $\beta_t^{-1} \sim 10^{-2}$. Thus it seems quite likely that a mean-field dynamo operating on fibril fields can produce flux tubes whose field strength locally exceeds turbulence-equipartition.

It is also possible that the fibril fields in the solar CZ produce an anisotropic viscoelastic medium. Since the present work provides the first formulation of fibril-field interactions we opted to treat the simplest case. We therefore assumed an isotropic distribution of flux tubes and ignored buoyancy. The result was a simple viscous strain involving a scalar coefficient of viscosity. Were the flux tubes aligned with a preferred direction, they would produce more strain in response to flows perpendicular to this: this viscous stress would involve a tensor coefficient. Indeed, their intrinsic buoyancy is likely to endow solar flux tubes with a radial preference, and large-scale orientation (Hale's polarity law) will give them a toroidal preference. We expect that the result will be for the fibril field to distribute momentum most effectively along conical surfaces of constant latitude. If this turns out to be the case, then it might play a significant role in establishing the observed pattern of differential rotations, in which conical surfaces co-rotate.

There is one other reason to expect strong anisotropy of the field that arises from the viscoelastic nature of the fibril medium. In viscoelastic fluid flow, another dimensionless number, the *Weissenberg number*, arises from the product of the shear rate and the characteristic relaxation time of the stress. When $\dot{\gamma}\tau_G$ is small, fibril structure is perturbed only marginally from its equilibrium statistical average, so apart from effects such as buoyancy,

will be nearly isotropic. However, when this number is large, flux tubes are strongly convected by the flow in a mean relaxation time, and will therefore be strongly anisotropic. In the entangled limit, the values of τ_G that arise from our physical estimates would indeed lead to large Weissenberg-number flows at shear rates characteristic of the CZ. This opens up the possibility of other phenomena from non-linear viscoelastic fluid dynamics such as elastic instability and strong "normal stresses" (Doi and Edwards 1986).

We thank Dr. Mark Linton for useful discussions on the reconnection of flux tubes, and the anonymous referee for helpful comments on the manuscript. This work was performed at the Institute for Theoretical Physics which is supported by the National Science Foundation Under Grant No. PHY99-07949. This work was supported by the DoD/AFOSR MURI grant "Understanding Magnetic Eruptions on the Sun and their Interplanetary Consequences".

REFERENCES

Batchelor, G. K. 1967, *Introduction to Fluid Dynamics*, Cambridge Univ. Press, Cambridge.

Bhattacharjee, A. and Yuan, Y. 1995, ApJ 449, 739.

Bird, B. R., Armstrong, R. C., and Hassager, O. 1987, *Dynamics of Polymeric Fluids. Vol. 1 Fluid mechanics*, John Wiley and Sons.

Böhm-Vitense, E. 1958, ZAp 46, 108.

Brown, S., Lenczycki, T., and Szamel, G. 2001, Phys. Rev. E 63, 052801.

Brummell, N., Cline, K., and Cattaneo, F. 2002, MNRAS 329, L73.

Caligari, P., Moreno-Insertis, F., and Schüssler, M. 1995, ApJ 441, 886.

Cates, M. and Deutsch, J. 1986, J. Phys. (Paris) 47, 2121.

Cheng, J. 1992, A&A 264, 243.

Choudhuri, A. R. 1990, A&A 239, 335.

Choudhuri, A. R. and Gilman, P. A. 1987, ApJ 316, 788.

Colby, R. and Rubinstein, M. 1990, Macromolecules 23, 2753.

DeLuca, E. E., Fisher, G. H., and Patten, B. M. 1993, ApJ 411, 383.

Doi, M. and Edwards, S. F. 1986, *The Theory of Polymer Dynamics*, Clarendon Press.

D'Silva, S. and Choudhuri, A. R. 1993, A&A 272, 621.

D'Silva, S. and Howard, R. F. 1993, Solar Phys. 148, 1.

Everaers, R. 1998, Eur. Phys. J. B 4, 341.

Fan, Y., Fisher, G. H., and DeLuca, E. E. 1993, ApJ 405, 390.

Fan, Y., Fisher, G. H., and McClymont, A. N. 1994, ApJ 436, 907.

Fetters, L., Lohse, D., Milner, S., and Graessley, W. 1999, Macromolecules 32, 6847.

Fisher, G. H., Fan, Y., Longcope, D. W., Linton, M. G., and Pevtsov, A. 2000, Solar Phys. 192, 119.

Jackson, J. D. 1975, *Classical Electrodynamics*, Wiley, New York.

Krause, F. and Rädler, K.-H. 1981, *Mean Field Magnetohydrodynamics*, Pergamnon Press.

Kulsrud, R. M. and Anderson, S. W. 1992, ApJ 396, 606.

Landau, L. D. and Lifshitz, E. M. 1986, *Theory of Elasticity*, Butterworth-Heinemann, 3rd edition.

Lin, H. and Rimmele, T. 1999, ApJ 514, 448.

Linton, M. G., Dahlburg, R. B., and Antiochos, S. K. 2001, ApJ 553, 905.

Longcope, D. W. and Choudhuri, A. R. 2002, Solar Phys. 205, 63.

Longcope, D. W. and Fisher, G. H. 1996, ApJ 458, 380.

Longcope, D. W., Fisher, G. H., and Pevtsov, A. A. 1998, ApJ 507, 417.

Matthews, P., Hughes, D., and Proctor, M. 1995, ApJ 448, 938.

McLeish, T. 2002, Adv. Phys. , In press.

Moffatt, H. K. 1978, *Magnetic Field Generation in Electrically Conducting Fluids*, Cambridge University Press, Cambridge.

Moreno-Insertis, F. and Emonet, T. 1996, ApJ 472, L53.

Nordlund, A., Brandenburg, A., Jennings, R. L., Rieutord, M., Ruokolainen, J., Stein, R. F., and Tuominen, I. 1992, ApJ 392, 647.

Obhukov, S., Rubinstein, M., and Duke, T. 1994, Phys. Rev. Lett. 73, 1263.

Ogilvie, G. I. 2001, MNRAS 325, 231.

Parker, E. N. 1955, ApJ 121, 491.

Parker, E. N. 1979, ApJ 230, 914.

Parker, E. N. 1984, ApJ 283, 343.

Roberts, B. and Webb, A. R. 1978, Solar Phys. 56, 5.

Roovers, J. 1988, Macromolecules 21, 1517.

Rubinstein, M. 1986, Phys. Rev. Lett. 57, 3023.

Schrijver, C. J., Title, A. M., Van Ballegooijen, A. A., Hagenaar, H. J., and Shine, R. A. 1997, ApJ 487, 424.

Spruit, H. C. 1974, Solar Phys. 34, 277.

Spruit, H. C. 1981, A&A 98, 155.

Stenflo, J. O. 1973, Solar Phys. 32, 41.

Vainshtein, S. I. and Cattaneo, F. 1992, ApJ 393, 165.

Weiss, N. O. 1966, Proc. Roy. Soc. A 293, 310.